Available online at www.sciencedirect.com
ScienceDirect
Intermetallics 15 (2007) 506–519
Intermetallics
www.elsevier.com/locate/intermet

Experimental study and thermodynamic calculation of Al–Mg–Sr phase equilibria

A. Janz [a], J. Gröbner [a], D. Mirković [a], M. Medraj [b], Jun Zhu [c], Y.A. Chang [c], R. Schmid-Fetzer [a,*]

[a] Clausthal University of Technology, Institute of Metallurgy, Robert-Koch-Strasse 42, D-38678 Clausthal-Zellerfeld, Germany
[b] Mechanical Engineering Department, Concordia University, 1455 de Maisonneuve Boulevard H549, Montreal, PQ, Canada H3G 1M8
[c] Department of Materials Science and Engineering, University of Wisconsin, 1509 University Avenue, Madison, WI 53706, USA

Received 10 May 2006; received in revised form 1 September 2006; accepted 4 September 2006
Available online 16 October 2006

Abstract

Selected samples of ternary Al–Mg–Sr alloys were investigated using thermal analysis, scanning electron microscopy and electron microprobe analysis. Additional samples, prepared in Montreal, were re-evaluated by simulation of their X-ray diffraction spectra and by careful analysis of their thermal analysis signal curves. A comprehensive and consistent thermodynamic description for the ternary Al–Mg–Sr system is generated by assessing all experimental data from the literature combined with the present experimental results. Extended ternary solid solubilities of binary phases and one ternary intermetallic phase are established in this system. Calculated phase diagram sections and the liquidus surface together with thermodynamic equilibrium and non-equilibrium Scheil calculations of selected alloys are used to demonstrate the good agreement with all of the experimental microstructures. This provides additional support for the thermodynamic description generated in this work.

Keywords: A. Ternary alloy systems; B. Phase diagrams; B. Thermodynamic and thermochemical properties; E. Phase diagram, prediction; F. Electron microscopy, scanning

1. Introduction

The commercial use of magnesium alloys is currently focused on Mg–Al-based alloys, especially on the AZ and AM series. These alloys combine good room temperature strength and ductility with satisfying salt-spray corrosion resistance and excellent castability. Special automotive applications, such as powertrain components or engine blocks, require sufficient creep resistance at elevated temperatures. For these elevated temperature applications, new alloys were developed by using additions of rare earth (RE) elements or Ca and Sr. The potential of these alloys was discussed by Luo [1]. He demonstrates promising results on the high temperature strength for Mg-based alloys with Sr and Ca, but emphasized the need for careful controlling to avoid castability problems like sticking and cracking. Additions of RE elements show similar advantages, but should be minimized considering their high cost. Baril et al. [2] studied creep resistance, mechanical properties and microstructure of magnesium alloys with less than 7 wt% Al and 3 wt% Sr. They report good creep resistance and excellent castability for such alloys, showing a microstructure consisting of a lamellar phase Al_4Sr at the grain boundaries of primary magnesium, (Mg). For higher Sr/Al ratio, a ternary phase is reported [3]. Formation of the $\gamma(Al_{12}Mg_{17})$-phase is only observed at lower Sr/Al ratio. The microstructure evolution of an Mg–5Al–2Sr (wt%) alloy during semisolid molding was studied by Czerwinski and Zielinska-Lipiec [4].

* Corresponding author.
E-mail address: schmid-fetzer@tu-clausthal.de (R. Schmid-Fetzer).

0966-9795/$ - see front matter © 2006 Elsevier Ltd. All rights reserved.
doi:10.1016/j.intermet.2006.09.001

These studies on promising applications emphasize the need for a precise thermodynamic description of the phase diagram of the ternary system Al–Mg–Sr. This is an important basis for a purposeful alloy development, enabling solidification calculations and the understanding of microstructures of promising alloys for various applications. The first thermodynamic calculation of the ternary system by Chartrand and Pelton [5] was limited to an extrapolation from the binary subsystems. The early experimental work of Makhmudov et al. [6–10] will be discussed in detail below. Numerous samples in the entire Al–Mg–Sr system were recently investigated by Parvez et al. [11] using DSC, XRD and metallography. The original experimental data of Parvez et al. [11] are critically re-assessed in the present work in cooperation with that group and are actually used for preliminary thermodynamic calculations in order to select the key samples studied here. The results of a recent study on the Mg-rich corner of the Mg–Al–Sr system by Cao et al. [12] are also implemented in this work. The purpose of this work is to generate a comprehensive and consistent thermodynamic description of the phase equilibria based on the new experimental data obtained in this work together with the bulk of, partly re-assessed, experimental literature data.

2. Experimental data from the literature

The early experimental information of the ternary Al–Mg–Sr system is from several publications of the group of Makhmudov and coworkers from Dushanbe, Tajikistan [6–10]. Although these papers on the ternary Al–Mg–Sr system all originate from the same group, several discrepancies can be observed.

The first paper [6] reports solubility limits at 400 °C for Mg-rich and Al-rich alloys derived by measurement of the variation of lattice parameter and microhardness with composition and metallographic identification of the phases. Alloys were synthesized in a resistance furnace in corundum crucible in an atmosphere of helium. Homogenization was performed in silica ampoules at 400 °C during 240 h. A ternary compound "X" in equilibrium with $Mg_{17}Sr_2$, γ and (Mg) was assumed by Makhmudov et al. [6], but not confirmed in Ref. [8]. Discrepancies between these two papers also concern the (Al) + Al_4Sr two-phase region and ternary solubilities in the binary Mg–Sr and Al–Sr compounds. No comment is made by Ref. [8] on these discrepancies. Partial liquidus surfaces of the Mg- and Al-corners were reported by Ref. [7] using differential thermal, microstructural and X-ray diffraction analysis and microhardness measurements. Two ternary eutectics were found, corresponding to E2 and U7 in the present notation.

The isothermal section at 400 °C, investigated by X-ray diffraction and microhardness measurements, is given by Ref. [8]. Large ternary solubilities of the binary phases were observed and confirmed by the variation of the lattice parameters. A ternary compound S in the Sr-rich corner, approximating to Al_6MgSr_{10}, was detected by Ref. [10]. Since its crystal structure has not been determined, the possibility of it being a ternary solubility of Mg in an Al_2Sr_3 phase was mentioned; that phase, Al_2Sr_3 is, however, not accepted as stable compound in the binary Al–Sr [9] examined the sections γ-$Mg_{17}Sr_2$, β-$Mg_{17}Sr_2$, Mg_2Sr–Al_4Sr, $Mg_{17}Sr_2$–Al_4Sr and β-Al_4Sr by DTA, X-ray diffraction analysis, metallography and microhardness measurements. They *assumed* all sections to be pseudobinary eutectic systems. The solubility limits at 300 and 400 °C were determined after annealing alloys for 300 h and water quenching. These solubilities do not agree with the 400 °C isothermal section given by Ref. [8] because these vertical sections are not aligned with all the tie-line directions and, thus, they are not "pseudobinary systems". Liquidus temperatures of 26 ternary alloys investigated by DTA were reported in Ref. [10]. For Sr-rich alloys the temperatures and liquid compositions of six invariant reactions were given in the Sr–Mg_2Sr–Al_4Sr partial ternary system. Unfortunately, Makhmudov et al. [10] did not tabulate the results of the DTA experiments. Again a ternary phase S in the Sr-rich region was reported.

A critical evaluation and thermodynamic calculation of the related binary subsystems was given by Ref. [5]. The ternary literature was mentioned, but the ternary phase diagram was only extrapolated from binary data using the quasi-chemical model for the liquid phase. The key feature of this ternary system, that is the formation of substantial ternary solid solutions or compounds, was not taken into account. The calculated phase equilibria and triangulation of the ternary system does not follow those determined experimentally by Makhmudov et al. [6–10].

In one of the commercial Mg–Al–Sr alloys, AJ52x, investigated by Baril et al. [2] precipitates were found and claimed to be a ternary phase with unclear stoichiometry, tentatively named $Al_3Mg_{13}Sr$ or $Mg_{68.3}$–Al_{17}–$Sr_{14.7}$ (wt%).

More recent experimental results are presented by Parvez et al. [11]. These data are carefully re-evaluated in cooperation with that group, based on the complete raw experimental information, and included in the present work. Part of these data required a substantial re-interpretation as detailed later.

In an investigation of phase equilibria in the Mg-rich corner the results of five samples are presented by Cao et al. [12]. Information was given on the primary phases observed and on the results of three samples annealed at 400 °C and investigated with SEM/BSE and EPMA.

3. Experimental investigations

3.1. Sample preparation

Within this work, seven new key samples were selected on the basis of preliminary thermodynamic calculations to provide relevant missing information on the Mg–Al–Sr phase equilibria. Samples denoted as C1–C7 are the new samples prepared in Clausthal, samples 01–21 are re-assessed samples from Montreal [11]. The first sample C1 should represent a commercial alloy ("AJ62") in the Mg-rich corner, the other six samples C2–C7 were placed on the section $Mg_{65}Al_{35}$–Sr (wt%) to investigate three-phase equilibria and the ternary

solubilities of the involved phases and to get additional information like liquidus data and the primary crystallizing phase.

The samples compositions are given in Table 1, sample C3 was destroyed during testing. Samples were prepared from Mg granules (99.98 wt%, Alfa, Karlsruhe, Germany), Al pieces (99.999/99.997 wt%, Alfa, Karlsruhe, Germany) and Sr pieces (99.99%, Aldrich-APL, Urbana, IL). All purity designations are related to the metal basis. The weighed materials were pressed carefully to pellets which were sealed in Ta-capsules by careful electric arc welding under argon at 1 bar.

After testing the tightness of the Ta-capsules in a separate furnace, differential thermal analysis was carried out using a Setaram MHTC 96 (Setaram, Caluire, France) Differential Scanning Calorimeter (DSC). The DSC measurements were carried out with heating/cooling rates of 5 and 1 K/min in three repeated cycles each. The temperature range of each cycle was typically 300–800 °C. A typical sample weight was about 250 mg. The overall uncertainty of DSC measurements was estimated as ±3 K for temperature determination.

After thermal analysis the samples were prepared metallographically. Care must be taken of the reactivity of the samples with oxygen which increased drastically with Sr-content. Therefore, ethanol had to be used for grinding and polishing with strictly limited time. As a consequence, not all scratches in the micrographs could be removed, as will be shown later.

The microstructure was investigated with scanning electron microscopy mostly using back scattered electrons (SEM/BSE) and local compositions were analyzed with electron probe microanalysis (EPMA) using a CAMECA SX100 (Cameca, France).

3.2. Experimental results

The results of the DSC analysis of the six samples of this work prepared in Clausthal are presented in Table 1. The last column shows the interpretation as obtained from the present thermodynamic calculation for the individual alloys.

Microstructures of most representative samples for the ternary system are shown in Fig. 1a–e. Phase identification was based on local chemical composition as measured by EPMA. Detailed analysis and interpretation of the solidification sequence of these microstructures will be given in Section 5, considering also the results of the thermodynamic calculations. It is noted that the Sr-richest sample, C7, was very brittle and difficult to investigate. For the other samples with less Sr-content, reasonably clear morphology could be obtained after proper preparation, as can be seen in the examples in Fig. 1.

An EPMA X-ray map of the two-phase (Mg) + γ-$Mg_{17}Al_{12}$ region in sample C2, Fig. 1d, is shown in Fig. 2. The key finding here is the negligible Sr-solubility in *both* phases, (Mg)

Table 1
Temperatures extracted from the DSC curves obtained by thermal analysis in the Al–Mg–Sr system for samples prepared in *Clausthal* and their interpretation

Nr.	Sample composition (wt%)	Thermal signal (°C)			Interpretation
		Heating[a]	Cooling[b]	Evaluated temperature	Calculated temperature (°C); phase boundary or **invariant reaction**
C1	$Mg_{92}Al_6Sr_2$	610	610	610	601 $L/L + (Mg)$
		546 w	537 w	546	544 $L + (Mg)/L + (Mg) + Mg_{17}Sr_2$
		521 s	516 s	521	**527 U4**
C2	$Mg_{58.5}Al_{31.5}Sr_{10}$	603	604	604	617 $L/L + Al_4Sr$
		482 w		482	488 $L + Al_4Sr/L + Al_4Sr + (Mg)$
		474 w	478 s	476	**477 U5**
			465 w	465	458 $L + (Mg) + \tau/(Mg) + \tau$
		438 s	433 s	438	**436 E4**
C4	$Mg_{45.5}Al_{24.5}Sr_{30}$	672	668	670	665 $L/L + Al_4Sr$
		577 s	566	577	595 $L + Al_4Sr/L + Al_4Sr + (Mg)$
		521 w	518 s	521	**527 U4**
C5	$Mg_{39}Al_{21}Sr_{40}$	653	651	652	652 $L/L + Al_4Sr$
					649 $L + Al_4Sr/L + Al_4Sr + Al_2Sr$
		607 s	601 n.c.	607	**595 E1**
		577 s	575 s	577	**582 $Al_2Sr + Mg_{17}Sr_2 = Al_4Sr + Mg_{38}Sr_9$**
C6	$Mg_{26}Al_{14}Sr_{60}$	668	669	668	708 $L/L + Al_2Sr$ (Mg_2Sr)
		not detec.	650 w	650	
		620 w	not detec.	620	625 $L + Mg_2Sr/L + Mg_2Sr + Al_2Sr$
		619 s	601 s	618	**611 U1**
C7	$Mg_{18.2}Al_{9.8}Sr_{72}$	634	632	633	676 $L/L + Mg_2Sr$
		513 s	not detec.	513	?
		480 w	482 s	480	?
		422 s	420 s	422	422 $L + Mg_2Sr/L + Mg_2Sr + Al_3Sr_8$

Invariant reactions were recognized from the peak shape.
w, weak and diffuse signal; s, strong and clear signal; not detec., not detected; n.c., not certain; ?, not assigned.
[a] Onset for invariant reactions, peak maximum otherwise.
[b] Onset.

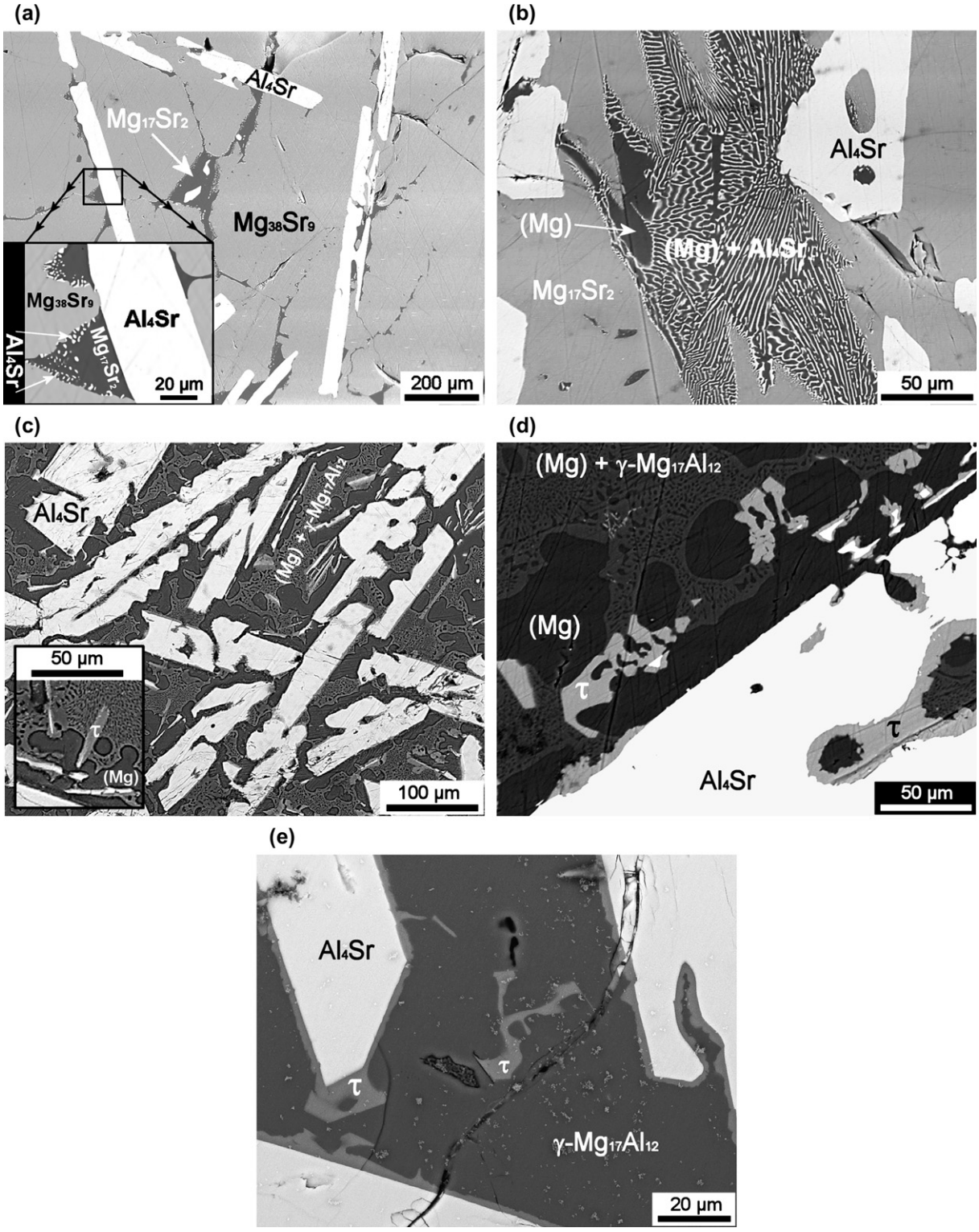

Fig. 1. Scanning electron micrographs (SEM/BSE) of five important samples, marked in Fig. 5, after slow cooling in DSC. (a) $Mg_{39}Al_{21}Sr_{40}$ (sample C5); inset shows a higher magnification. (b) $Mg_{45.5}Al_{24.5}Sr_{30}$ (sample C4). (c) $Mg_{43.8}Al_{33.6}Sr_{22.6}$ (sample 06); inset shows a higher magnification. (d) $Mg_{58.5}Al_{31.5}Sr_{10}$ (sample C2). (e) $Mg_{30}Al_{46}Sr_{24}$ (sample 08).

and γ-$Mg_{17}Al_{12}$. The measured maximum ternary solubilities from EPMA are given in the second last column of Table 2. The large primary grown Al_4Sr-bars, such as the one in Fig. 1d, show no variation in composition from center to edge, according to a line-scan over such a particle.

The ternary phase τ was clearly identified in sample C2 (Fig. 1d) with an approximate content of ~13.5 wt% Sr based on EPMA data, thus differing significantly from the γ-$Mg_{17}Al_{12}$ phase. The EPMA measurement of τ gives 46.5 wt% Mg and 40 wt% Al. This measured Mg/Al ratio of

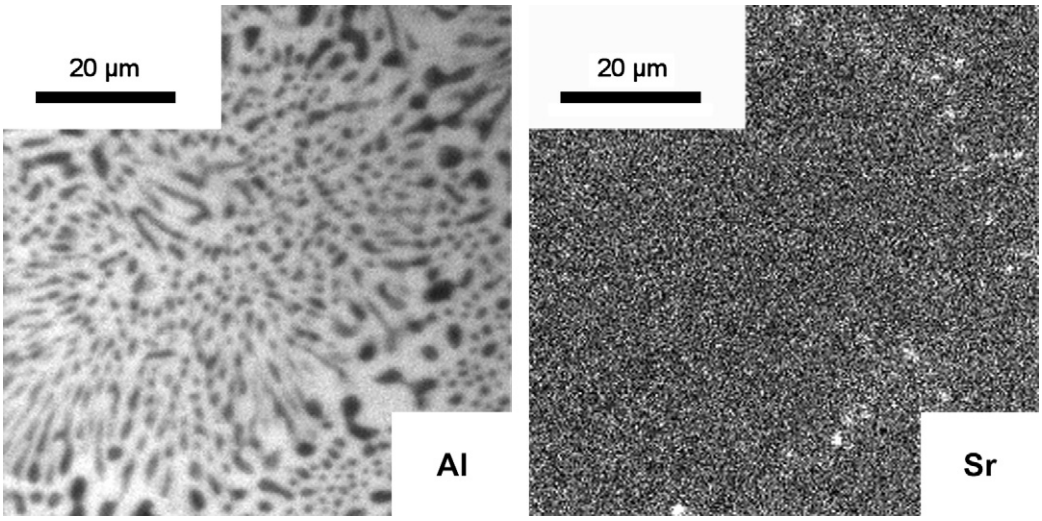

Fig. 2. X-ray mapping of an (Mg) + γ-$Mg_{17}Al_{12}$-region in sample C2. The left picture shows the Al-content (max. 800 counts, bright areas are γ-$Mg_{17}Al_{12}$, dark areas are (Mg)) and right picture shows the Sr-content (max. 8 counts).

Table 2
All solid phases of the Al–Mg–Sr system and ternary solubilities of binary compounds

Phase/temperature range (°C)	Pearson symbol/prototype	Lattice parameters (pm)	Ref.	Ternary solubility (wt%)		
				Experimental		Calculated (this work)
				[8]	(This work)	
(Al)/<660	cF4/Cu	$a = 404.96$ pure Al at 25 °C	[21]			
(Mg)/<650	hP2/Mg	$a = 320.94$ $c = 521.07$ pure Mg at 25 °C	[21]			
αSr/<556	cF4/Cu	$a = 608.4$ pure αSr at 25 °C	[21]			
βSr/547–777	cI2/W	$a = 487$ pure βSr at 614 °C	[21]			
$Mg_{17}Sr_2$/<605	hP38/Th_2Ni_{17}	$a = 1053.0$ to 1031.0 $c = 1040.8$ to 1019.0	[8]	11.6 Al	16.5 Al	16.3 Al
$Mg_{38}Sr_9$/<601	hP94/Sr_9Mg_{38}	$a = 1050.0$ $c = 2825.1$	[5]		16.8 Al	16.3 Al
$Mg_{23}Sr_6$/<614	cF116/Th_6Mn_{23}	$a = 1503$ to 1463.5	[8]	21.2 Al	15.9 Al	14.6 Al
Mg_2Sr/<713	hP12/$MgZn_2$	$a = 647.5$ to 635.2 $c = 1043.0$ to 1034.5	[8]	6.2 Al	12.9 Al	11.5 Al
Al_4Sr/<1021	tI10/$BaAl_4$	$a = 446.3$ to 448.5 $c = 1107.0$ to 1131.0	[8]	17.0 Mg	10.2 Mg	10.2 Mg
Al_2Sr/<922	oI12/$CeCu_2$	$a = 480.2$ to 480.9 $b = 791.2$ to 794.3 $c = 796.5$ to 804.0	[8]	11.3 Mg	17.9 Mg	18.0 Mg
Al_7Sr_8/<668	cP64/Sr_8Al_7	$a = 1275.3$	[5]		~1 Mg	Nil
Al_3Sr_8/342–605	aP22/Ca_8In_3		[15]			Nil
β, Al_3Mg_2/<451	cF1832/Mg_2Al_3	$a = 2823.9$	[22]		<1 Sr	Nil
ε, $Al_{30}Mg_{23}$/250–410	hR53/$Mg_{23}Al_{30}$	$a = 1282.54$ $c = 2174.78$	[20]		<1 Sr	Nil
γ, $Al_{12}Mg_{17}$/<464	cI58/αMn	$a = 1054.38$	[20]		<1 Sr	Nil
τ, $Al_{38}Mg_{58}Sr_4$/<477	Not certain		(This work)			

τ is very similar to that of γ-$Mg_{17}Al_{12}$. The fact that τ is a distinct ternary phase and not the suspected ternary solubility of γ-$Mg_{17}Al_{12}$ is further compounded by the marked contrast in the SEM/BSE micrographs in Fig. 1d and e, indicating a two-phase structure of τ + γ-$Mg_{17}Al_{12}$.

All of the original experimental data from samples prepared in Montreal, including unpublished SEM and EPMA data, were used for this work. The data which were partly previously published [11] were critically re-assessed in detail. This included both the raw XRD-patterns as well as the raw thermal analysis DSC signal curves. The entity of this DSC data was re-assessed with the objective to obtain both higher accuracy and proper information on the type of reaction. Some samples had to be dismissed due to inconsistencies between heating and cooling cycles. The results are shown in Table 3, with the present interpretation from the calculation in the same format as in Table 1.

Information on all solid phases of the Al–Mg–Sr system is compiled in Table 2. The crystallographic data are from the literature. The ternary solubilities determined in this work by experiment and/or calculations are compared with the experimental data of Ref. [8]. Large solubilities of the third component up to 18 wt% are observed in nearly all Sr-containing binary phases. The ternary phase τ found in this work is given with its approximated atomic composition, $Al_{38}Mg_{58}Sr_4$.

Reassessment of the XRD phase analysis data partly published in Ref. [11] was done comparing the entity of raw XRD-patterns with calculated spectra obtained using the software PowderCell 2.4 [13]. It was possible to reproduce nearly all of the peaks in the XRD-patterns by adjusting the lattice parameters of the binary phases slightly, assuming extended ternary solubilities. Doing so, most of the proposed ''ternary phases'' [11] could be explained as ternary solubilities of known binary phases. The ternary solubilities obtained during this evaluation are in qualitative agreement with the more precise information measured with EPMA, which is given in Table 2. This information, together with the aggregated thermal analysis data in Tables 1 and 3, forms the basis of the current thermodynamic modeling. The experimental information gathered from the microstructures, regarding phase formation and primary phases, had been used as an independent check as discussed in Section 5.

4. Thermodynamic modeling

The present modeling of the ternary phase equilibria is based on the published binary thermodynamic data sets of the subsystems Al–Mg [14], Al–Sr (version 1 with random solution model and including the compound Al_3Sr_8) [15] and Mg–Sr [16].

The Gibbs energy function $G_i^{0,\phi}(T) = G_i^{\phi}(T) - H_i^{\mathrm{SER}}$ for the element i (i = Al, Mg, Sr) in the ϕ phase (ϕ = fcc (Al, αSr), bcc (βSr), hcp (Mg), and liquid) is described by the equation:

$$G_i^{0,\phi}(T) = a + bT + cT\ln T + dT^2 + eT^3 + fT^{-1} + gT^7 + hT^{-9} \tag{1}$$

where H_i^{SER} is the molar enthalpy of the stable element reference (SER) at 298.15 K and 1 bar, and T is the absolute temperature. The Gibbs energy functions for Al, Mg and Sr are taken from the SGTE compilation of Dinsdale [17].

The liquid, fcc (Al, αSr), bcc (βSr) and hcp (Mg) solution phases are described by the disordered substitutional solution model. For the phase, ϕ the molar Gibbs energy is expressed by the following equation:

$$G^{\phi} = \sum_{i=1}^{3} x_i G_i^{0,\phi} + RT\sum_{i=1}^{3} x_i \ln x_i + {}^{E}G^{\mathrm{bin},\phi} + {}^{E}G^{\mathrm{tern},\phi} \tag{2}$$

where R is the gas constant, and x_i is the molar fraction of i = Al, Mg and Sr. All excess contributions originating from all the binary interactions (${}^{\mathrm{E}}G^{\mathrm{bin}}$) or ternary interactions (${}^{\mathrm{E}}G^{\mathrm{tern}}$) are:

$${}^{E}G^{\mathrm{bin},\phi} = \sum_{i=1}^{2}\sum_{j>i}^{3} x_i x_j \sum_{v=0}^{n} L_{ij}^{v,\phi}\left(x_i - x_j\right)^{v} \tag{3}$$

$${}^{E}G^{\mathrm{tern},\phi} = x_1 x_2 x_3\left\{L_{123}^{0,\phi}x_1 + L_{123}^{1,\phi}x_2 + L_{123}^{2,\phi}x_3\right\} \tag{4}$$

The ternary interaction parameters $L_{123}^{v,\phi}$ may be linearly temperature dependent and are optimized together with all experimental data concerning the ϕ phase. Ternary parameters were only used for the liquid phase in this system. Specifically, only one parameter $L_{123}^{1,\mathrm{Liquid}}$ was used for an asymmetric modeling of the ternary liquid phase. The other parameters, $L_{123}^{0,\mathrm{Liquid}}$ and $L_{123}^{2,\mathrm{Liquid}}$ were taken as zero. Eqs. (2) and (3) without ternary parameters correspond to a Redlich–Kister/Muggianu type extrapolation from the binary sets, which was chosen for the sake of simplicity.

The six binary phases $Mg_{17}Sr_2$, $Mg_{38}Sr_9$, $Mg_{23}Sr_6$, Mg_2Sr, Al_4Sr and Al_2Sr exhibit ternary solution ranges, forming line compounds. Since all ternary solubilities extend only at constant strontium content, Sr becomes the only constituent on the second sublattice of these phases. They were modeled with two sublattices and a substitutional solution on the first sublattice, such as (Al,**Mg**)$_{17}Sr_2$, (Al,**Mg**)$_{38}Sr_9$, (Al,**Mg**)$_{23}Sr_6$ and (**Al**,Mg)$_4$Sr. The bold type denotes the majority species. The phases Mg_2Sr and Al_2Sr were modeled as separate phases because of their different crystal structure, using (Al,**Mg**)$_2$Sr and (**Al**,Mg)$_2$Sr. The Gibbs energy of these phases (Al,Mg)$_m$Sr$_n$ (per mole of formula) is expressed in the Compound-Energy Formalism [18] by

$$G^{\phi} = y_{\mathrm{Al}}G_{\mathrm{Al:Sr}}^{0,\phi} + y_{\mathrm{Mg}}G_{\mathrm{Mg:Sr}}^{0,\phi} + mRT\left(y_{\mathrm{Al}}\ln y_{\mathrm{Al}} + y_{\mathrm{Mg}}\ln y_{\mathrm{Mg}}\right) + y_{\mathrm{Al}}y_{\mathrm{Mg}}\left(L_{\mathrm{Al,Mg:Sr}}^{0,\phi}\right) \tag{5}$$

where y_{Al} and y_{Mg} are the site fractions of Al and Mg on the first sublattice. The parameters $L_{\mathrm{Al,Mg:Sr}}^{0,\phi}$ describe ternary interactions essentially within the sublattice. The parameters $G_{\mathrm{i:Sr}}^{0,\phi}$, i = Al or Mg, are also called compound energies and describe interactions essentially between the sublattices. The parameters $G_{\mathrm{Mg:Sr}}^{0,\phi}$ for the stable binary Mg–Sr phases (ϕ = $Mg_{17}Sr_2$,

Table 3
Temperatures extracted from the DSC curves obtained by thermal analysis in the Al–Mg–Sr system in *Montreal* and their interpretation in the present work

Nr.	Sample composition (wt%)	Thermal signal (°C)			Interpretation
		Heating[a]	Cooling[b]	Evaluated temperature	Calculated temperature (°C); phase boundary or **invariant reaction**
01	$Al_{8.0}Mg_{88.5}Sr_{3.5}$	605 s	596 s	600	601 $L/L + (Mg)$
		530 w	–	530	544 $L + (Mg)/L + (Mg) + Mg_{17}Sr_2$
		527 s	524 s	527	**527 U4**
04	$Al_{27.7}Mg_{65.6}Sr_{6.7}$	–	–	not detec.	567 $L/L + Al_4Sr$
		–	524 w	524	498 $L + Al_4Sr/L + Al_4Sr + (Mg)$
		476 w	475 w	476	**477 U5**
		442 s	435 w	442	**436 E4**
		–	427 s	–	?
05	$Al_{28}Mg_{52}Sr_{20}$	653 w	652 w	653	655 $L/L + Al_4Sr$
		513 s	510 s	510	500 $L + Al_4Sr/L + Al_4Sr + (Mg)$
		489 s	453 s	?	475 $L + Al_4Sr + (Mg)/Al_4Sr + (Mg)$
				–	472 $Al_4Sr + (Mg)/Al_4Sr + (Mg) + \tau$
		441 s	431 s	436	(E4 ?)
07	$Al_{40.1}Mg_{46.9}Sr_{13.0}$	–	661 w	661	687 $L/L + Al_4Sr$
		501 w	–	501 ?	476 $L + Al_4Sr/L + Al_4Sr + \tau$
		453 s	444 s	453	**460 U6**
		443 s	431 s	436	(E4 ?)
08	$Al_{46}Mg_{30}Sr_{24}$	499 s	–	–	800 $L/L + Al_4Sr$
		489 w	460 w	–	473 $L + Al_4Sr/L + Al_4Sr + \tau$
		457 s	445 s	457	**460 U6**
		438 w	430 w	–	?
10	$Al_{22.8}Mg_{54.4}Sr_{22.8}$	625 w	612 s	625	625 $L/L + Al_4Sr$
		560 s	544 s	560	581 $L + Al_4Sr/L + Al_4Sr + Mg_{17}Sr_2$
		523 s	513 s	523	**527 U4**
11	$Al_{28}Mg_{43}Sr_{29}$	–	–	–	694 $L/L + Al_4Sr$
		561 s	546 s	561	586 $L + Al_4Sr/L + Al_4Sr + Mg_{17}Sr_2$
		524 s	513 s	524	**527 U4**
13	$Al_{22.4}Mg_{41.4}Sr_{36.2}$	677 w	672 w	672	661 $L/L + Al_4Sr$
		–	–	–	597 $L + Al_4Sr/L + Al_4Sr + Mg_{17}Sr_2$
		597 s	583 s	597	**595 E1**
		581 s	568 s	581	**582 $Al_2Sr + Mg_{17}Sr_2 = Al_4Sr + Mg_{38}Sr_9$**
14	$Al_{29.4}Mg_{30.7}Sr_{39.9}$	–	–	–	746 $L/L + Al_4Sr$
		605 s	599 s	605	594 $L + Al_4Sr/Al_4Sr + Mg_{17}Sr_2 + Al_2Sr$
		579 s	570 s	579	**582 $Al_2Sr + Mg_{17}Sr_2 = Al_4Sr + Mg_{38}Sr_9$**
15	$Al_{50.5}Mg_{40}Sr_{9.5}$	492 ?	662	662 ?	703 $L/L + Al_4Sr$
		–	458 w	?	463 $L + Al_4Sr/L + Al_4Sr + \gamma$
		459 s	448 s	454	450 $L + Al_4Sr + \gamma/Al_4Sr + \gamma$
16	$Al_{59}Mg_{30}Sr_{11}$	670 w	670 w	670	748 $L/L + Al_4Sr$
		453 s	441 s	446	447 $L + Al_4Sr/Al_4Sr + \gamma + \beta$
		–	–	–	410 $Al_4Sr + \gamma + \beta/Al_4Sr + \gamma + \beta + \varepsilon$
18	$Al_{63.8}Mg_{31.6}Sr_{4.6}$	–	600 ?	–	674 $L/L + Al_4Sr$
		472 w	444 w	460	451 $L + Al_4Sr/L + Al_4Sr + \beta$
		452 s	442 s	452	**450 E2**
19	$Al_{87.2}Mg_{10.8}Sr_{2.0}$	–	–	–	614 $L/L + Al_4Sr$
		607 s	597 s	602	598 $L + Al_4Sr/L + Al_4Sr + (Al)$
		–	–	–	490 $L + Al_4Sr + (Al)/Al_4Sr + (Al)$
		455 s	442 s	455	(U7 ?)
20	$Al_{62}Mg_{15}Sr_{23}$	–	–	–	872 $L/L + Al_4Sr$
		505 w	497 w	–	?
		476 w	–	476	476 $L + Al_4Sr/L + Al_4Sr + (Al)$
		454 s	440 s	454	**450 E2**
21	$Al_{8.0}Mg_{70.5}Sr_{21.5}$	–	–	–	599 $L/L + Mg_{17}Sr_2$
		584 s	572 s	575	573 $L + Mg_{17}Sr_2/L + Mg_{17}Sr_2 + (Mg)$
		564 s	557 s	561	560 $L + Mg_{17}Sr_2 + (Mg)/Mg_{17}Sr_2 + (Mg)$

w, weak and diffuse signal; s, strong and clear signal; not detec., not detected;?, not assigned.
Invariant reactions were recognized from the peak shape.
[a] Onset for invariant reactions, peak maximum otherwise.
[b] Onset.

$Mg_{38}Sr_9$, $Mg_{23}Sr_6$, Mg_2Sr) were taken from the binary data set Mg–Sr [16]. For these solution phases, the parameters $G^{0,\phi}_{Al:Sr}$ represent the metastable end members of the solid solutions in the binary Al–Sr system. They were given sufficiently large positive values in this work. For the stable binary Al–Sr phases (Al_4Sr and Al_2Sr), the parameters $G^{0,\phi}_{Al:Sr}$ were taken from the binary data set Al–Sr [15] and the parameters $G^{0,\phi}_{Mg:Sr}$ represent the metastable end members of the solid solutions in the binary Mg–Sr system. The ternary interaction parameters $L^{0,\phi}_{Al,Mg:Sr}$ together with the compound energy parameters of the metastable end members were optimized in the present study using mainly the experimental data obtained in this work.

The binary phases β, ε and Al_7Sr_8 and the ternary phase τ were modeled as stoichiometric compounds referred to the stable elements as given for the example of τ, $Al_{38}Mg_{58}Sr_4$:

$$G^{\tau} = 38G^{0,fcc}_{Al}(T) + 58G^{0,hcp}_{Mg}(T) + 4G^{0,fcc}_{Sr}(T) + A^{\tau} + B^{\tau}T \qquad (6)$$

The parameters A^{τ} and $-B^{\tau}$ correspond to the enthalpy and entropy of formation. This Gibbs energy of formation parameter for the ternary phase τ was determined according to the observed solid state equilibria and the nonvariant reaction U5: $L + Al_4Sr = \tau + (Mg)$, which was measured at 476 °C.

In order to check if reasonable values are assigned to the parameters A^{τ} and B^{τ}, the absolute entropy and the entropy of fusion of τ were calculated. The absolute entropy of the phase τ at 298 K is $S^{0,\tau}_{298} = 26.92$ J/K mol-atoms, which is in a reasonable range compared with the data of the components. The negative entropy of formation, −5 J/K mol-atoms, is also not excessively large. The entropy of fusion at the metastable congruent melting point of τ (507.4 °C) is $\Delta_{fus}S(\tau) = 19.02$ J/K mol-atoms or 2.3 R. This is about twice as high as the values for typical fcc and hcp metals but still substantially below the values for strongly covalent elements, such as Ge or Si [17]. Lower values of $\Delta_{fus}S(\tau)$ could not be obtained during parameter optimization without deteriorating the overall quality of the description.

It is noted that the corresponding entropies of formation (negative B parameters) for the metastable end members of the solution phases $(Al,\mathbf{Mg})_{38}Sr_9$ and $(Al,\mathbf{Mg})_{23}Sr_6$, i.e. $(Al)_{38}Sr_9$ and $(Al)_{23}Sr_6$, are relatively high, about 17 J/K mol-atoms. Converting this to absolute entropies, relatively small but still acceptable values are obtained for these two metastable phases. The final parameter settings for the actually stable phases $(Al,\mathbf{Mg})_{38}Sr_9$, $(Al,\mathbf{Mg})_{23}Sr_6$ are a delicate balance resulting from the large Al-solubilities and maintaining a stable solid solution around 400 °C for these two adjacent and competing phases.

Results of the final thermodynamic modeling are summarized in the following calculated phase diagrams. The liquidus projection is shown in Fig. 3a with a detailed view of the Mg–Al-rich side in Fig. 3b. The corresponding calculated invariant reactions and maxima involving the liquid phase are listed in Tables 4a and b, respectively, and compared with the experimental temperatures. The optimized thermodynamic parameters are given in Table 5.

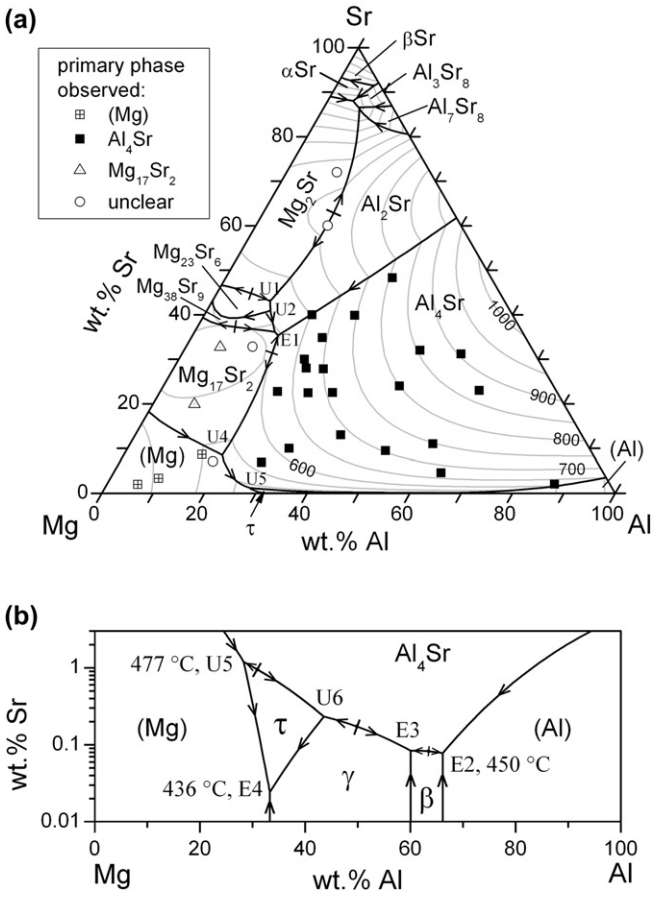

Fig. 3. Calculated liquidus projection of the Mg–Al–Sr system. (a) The black lines represent monovariant lines and the grey lines isotherms with an interval of 50 °C. The data points show compositions of samples with experimentally observed primary phases including data from Refs. [11,12]. (b) Detailed view of the Mg–Al side in logarithmic presentation.

5. Discussion

5.1. Comparison between experimental thermal analysis and EPMA data and the thermodynamic calculations

Superimposed in Fig. 3a are all the sample compositions prepared in Clausthal (see Table 1) and Montreal (see Table 3) and the five samples of Cao et al. [12]. The good agreement between the observed primary crystallizing phases and the calculation is noted. Generally, Al_4Sr is the dominating phase in this system. For Mg-rich alloys the primary fields of (Mg) and $Mg_{17}Sr_2$ are also supported by experimental data. The solidification sequence of alloys with primary (Mg)-matrix solidification may also involve the phases τ and γ, as detailed in Fig. 3b and discussed later.

The location of the pertinent solid phases is exposed in two calculated isothermal sections, Figs. 4 and 5. In both diagrams the substantial ternary solubilities of the binary phases are displayed with thick black lines; in Fig. 4 three-phase fields are highlighted in grey color. Calculated equilibria > 70 wt% Sr are not supported by ternary experimental data.

The ternary phase τ forms below 477 °C and is not present in the 500 °C section in Fig. 4. Two residual liquids are stable

Table 4a
Invariant four-phase reactions involving liquid phase in the ternary Al–Mg–Sr system

Type	T (°C) calculated	Reaction	T (°C) measured		T (°C) [7,9]
			Clausthal	Montreal	
U1	611	$L + Mg_2Sr = Al_2Sr + Mg_{23}Sr_6$	619		610 ?
U2	606	$Mg_{23}Sr_6 + Al_2Sr = Mg_{38}Sr_9 + L$			
U3	595.4	$L + Mg_{38}Sr_9 = Mg_{17}Sr_2 + Al_2Sr$			
E1	595.3	$L = Mg_{17}Sr_2 + Al_2Sr + Al_4Sr$	607	597	
D	555	$Al_3Sr_8 + \beta Sr = \alpha Sr + L$			
U4	527	$L + Mg_{17}Sr_2 = (Mg) + Al_4Sr$	521/519	527/524/523	
U5	477	$L + Al_4Sr = \tau + (Mg)$	473	476	
U6	460	$L + Al_4Sr = \tau + \gamma$		457/453	
E2	450	$L = Al_4Sr + (Al) + \beta$		454/452	445
E3	449	$L = Al_4Sr + \beta + \gamma$			
E4	436	$L = (Mg) + \gamma + \tau$	438	442	438
U7	427	$L + Al_2Sr = Mg_2Sr + Al_7Sr_8$			
U8	423	$L + Al_7Sr_8 = Mg_2Sr + Al_3Sr_8$			
E5	399	$L = Al_3Sr_8 + Mg_2Sr + \alpha Sr$			

at this temperature: one in the Sr-rich corner, the other close to the binary eutectic $L = (Mg) + \gamma\text{-}Mg_{17}Al_{12}$.

At 400 °C in Fig. 5 the τ phase appears and solidification of the Mg–Al-rich liquid is complete. Superimposed on this diagram are the measured chemical compositions of the investigated phases from EPMA (this work and [12]). These data compound the modeled negligible solubility of Sr in the Mg–Al binary solid phases. The ternary solid solution range of Al_4Sr is also reasonably well supported, considering experimental difficulties with increasing Sr-content. The same applies to the ternary solubility limit of $Mg_{23}Sr_6$ and $Mg_{38}Sr_9$, whereas a larger scatter is noted for the $Mg_{17}Sr_2$ phase with more data points falling into the adjacent three-phase field $Mg_{17}Sr_2 + (Mg) + Al_4Sr$. Overall, the triangulation of Ref. [8] with the dominating tie line from (Mg) to Al_4Sr is also in good agreement with the present thermodynamic calculations.

The samples C2–C7 in this work (Table 1) have been placed on the section $Mg_{65}Al_{35}$–Sr. The corresponding partial vertical section up to 80 wt% Sr is given in Fig. 6a. Superimposed are also the DSC results of samples 04 and 13 (Table 3), their compositions are close to this section. A good agreement of the calculation with the measured liquidus data up to 50 wt% Sr is noted. Also the invariant reactions are well reproduced by the thermodynamic modeling, such as the peritectic formation of the τ phase at 477 °C.

The thermodynamic modeling at more than 70 wt% Sr is only partly supported by the experimental data. The measured ternary solubilities of the binary phases, especially along the Mg_2Sr–Al_2Sr section, and the accepted Sr–Al and Sr–Mg binary descriptions essentially determine the thermodynamic calculation in the Sr-rich corner. There is not much room to shift the reaction temperatures in the calculation. This disagreement above 70 wt% Sr might be due to the existence of a ternary phase in this Sr-rich area as mentioned in Ref. [10]. Since the Sr-corner is not the main focus of this work, this problem will not be further addressed.

The second vertical section presented in Fig. 6b is calculated at constant 10 wt% Sr. Superimposed are the thermal signals of six samples with a composition close to this section. Most of these data show good agreement between calculated and measured invariant reactions. Around 665 °C a weak signal shows up in three samples between 40 and 60 wt% Al. For samples 15 and 16, a deviation from the calculated liquidus line is observed. The calculated liquidus, however, is strongly fixed by the extension of the smooth Al_4Sr liquidus surface in Fig. 3 and the well accepted binary liquidus lines.

Since many other samples cannot be shown on such vertical sections, a comparison of the calculated results with the experimental thermal analysis data was performed for each individual alloy in Tables 1 and 3. The result plotted in Fig. 7 shows a good agreement, especially for the invariant reactions. The deviating liquidus data at higher temperature are due to some artifacts in the measurement of some samples with higher Al-content, as discussed above for Fig. 6b, and for those with very high Sr-content.

5.2. Microstructures evolved during slow solidification

The most important solid state three-phase fields for Mg–Al-rich alloys in this ternary system are highlighted by characters (a)–(e) in the isothermal section given in Fig. 5. On the Al-rich side the three three-phase regions are quite simple due to the tie lines merging to virtually pure binary Al_4Sr. The phase formation in the regions (a)–(e) is discussed below, using the microstructures of five representative samples after

Table 4b
Invariant ternary three-phase reactions involving liquid phase in the Al–Mg–Sr system

Type	T (°C) calculated	Reaction
Max1	710	$L = Al_2Sr + Mg_2Sr$
Max2	614	$L = Mg_{23}Sr_6 + Mg_2Sr$
Max3	601	$L = Mg_{17}Sr_2 + Mg_{38}Sr_9$
Max4	598	$L = Al_4Sr + Mg_{17}Sr_2$
Max5	478	$L = Al_4Sr + \tau$
Max6	463	$L = Al_4Sr + \gamma$
Max7	452	$L = Al_4Sr + \beta$

Table 5
Ternary thermodynamic parameters for the Al–Mg–Sr system

Phase name	Model	Parameters in J/mol
Liquid	(Al,Mg,Sr)	$L^{0,\text{Liquid}}_{\text{Al,Mg,Sr}} = 0$ $L^{1,\text{Liquid}}_{\text{Al,Mg,Sr}} = -25\,000$ $L^{2,\text{Liquid}}_{\text{Al,Mg,Sr}} = 0$
$Mg_{17}Sr_2$	$(Al,\mathbf{Mg})_{17}Sr_2$	$G^{0,\text{Mg}_{17}\text{Sr}_2}_{\text{Al:Sr}} = -175\,000 + 50T + 17G^{0,\text{fcc}}_{\text{Al}} + 2G^{0,\text{fcc}}_{\text{Sr}}$ $L^{0,\text{Mg}_{17}\text{Sr}_2}_{\text{Al,Mg:Sr}} = -75\,400$
$Mg_{38}Sr_9$	$(Al,\mathbf{Mg})_{38}Sr_9$	$G^{0,\text{Mg}_{38}\text{Sr}_9}_{\text{Al:Sr}} = -1\,250\,000 + 180T + 38G^{0,\text{fcc}}_{\text{Al}} + 9G^{0,\text{fcc}}_{\text{Sr}}$ $L^{0,\text{Mg}_{38}\text{Sr}_9}_{\text{Al,Mg:Sr}} = -220\,000$
$Mg_{23}Sr_6$	$(Al,\mathbf{Mg})_{23}Sr_6$	$G^{0,\text{Mg}_{23}\text{Sr}_6}_{\text{Al:Sr}} = -750\,000 + 500T + 23G^{0,\text{fcc}}_{\text{Al}} + 6G^{0,\text{fcc}}_{\text{Sr}}$ $L^{0,\text{Mg}_{23}\text{Sr}_6}_{\text{Al,Mg:Sr}} = -190\,000$
Mg_2Sr	$(Al,\mathbf{Mg})_2Sr$	$G^{0,\text{Mg}_2\text{Sr}}_{\text{Al:Sr}} = -78\,600 + 19.8T + 2G^{0,\text{fcc}}_{\text{Al}} + G^{0,\text{fcc}}_{\text{Sr}}$
Al_4Sr	$(\mathbf{Al},Mg)_4Sr$	$G^{0,\text{Al}_4\text{Sr}}_{\text{Mg:Sr}} = -41\,000 + 50T + 4G^{0,\text{hcp}}_{\text{Mg}} + G^{0,\text{fcc}}_{\text{Sr}}$
Al_2Sr	$(\mathbf{Al},Mg)_2Sr$	$G^{0,\text{Al}_2\text{Sr}}_{\text{Mg:Sr}} = -31\,016 + 10T + 2G^{0,\text{hcp}}_{\text{Mg}} + G^{0,\text{fcc}}_{\text{Sr}}$ $L^{0,\text{Al}_2\text{Sr}}_{\text{Al,Mg:Sr}} = +900$
τ, $Al_{38}Mg_{58}Sr_4$	$(Al)_{38}(Mg)_{58}(Sr)_4$	$G^{0,\tau}_{\text{Al:Mg:Sr}} = -1\,050\,000 + 500T + 38G^{0,\text{fcc}}_{\text{Al}} + 58G^{0,\text{hcp}}_{\text{Mg}} + 4G^{0,\text{fcc}}_{\text{Sr}}$

slow solidification in the DSC as given in Fig. 1a–e. The sample compositions are approximately located at the corresponding characters in Fig. 5. It is noted that the calculated phase equilibria at room temperature indicate a significant reduction of ternary solubility only for the $Mg_{17}Sr_2$ phase. Focusing on the three-phase equilibria involving the (Mg) phase, fields (d) and (c) are also present at 25 °C, whereas field (b) is replaced by two three-phase regions, (Mg) + $Mg_{17}Sr_2$ + $Mg_{38}Sr_9$ and (Mg) + $Mg_{38}Sr_9$ + Al_4Sr.

In Fig. 1a (sample C5), we can see the three phases Al_4Sr, $Mg_{17}Sr_2$ and $Mg_{38}Sr_9$, which are, according to the thermodynamic calculation at 400 °C, in equilibrium in field (a) of Fig. 5. The shape of the large bars of Al_4Sr also supports the calculated primary precipitation. A more detailed view of the equilibrium solidification is given by the calculated phase fractions of this alloy in Fig. 8. It reveals secondary solidification of the (transient) phase Al_2Sr and additional formation of $Mg_{17}Sr_2$ in the ternary eutectic E1. This $Mg_{17}Sr_2$ reacts with Al_2Sr at 582 °C in the solid state reaction U9, $Mg_{17}Sr_2 + Al_2Sr = Al_4Sr + Mg_{38}Sr_9$, resulting in a complete consumption of Al_2Sr and the final equilibrium phase assembly $Mg_{17}Sr_2 + Al_4Sr + Mg_{38}Sr_9$. It is noteworthy that this solid state transition type reaction U9 at 582 °C obviously runs to completion since no trace of unreacted Al_2Sr could be found in the microstructure. It is also interesting that the calculated phase growth of Al_4Sr is negligible in the ternary eutectic E1 but noticeable in the solid state reaction U9. This is supported by the fact that Al_4Sr also occurs as very small particles within the $Mg_{17}Sr_2$-field, shown in the magnified inset in Fig. 1a.

The microstructure of sample C4, shown in Fig. 1b, also displays the three equilibrium phases $Mg_{17}Sr_2 + Al_4Sr + (Mg)$

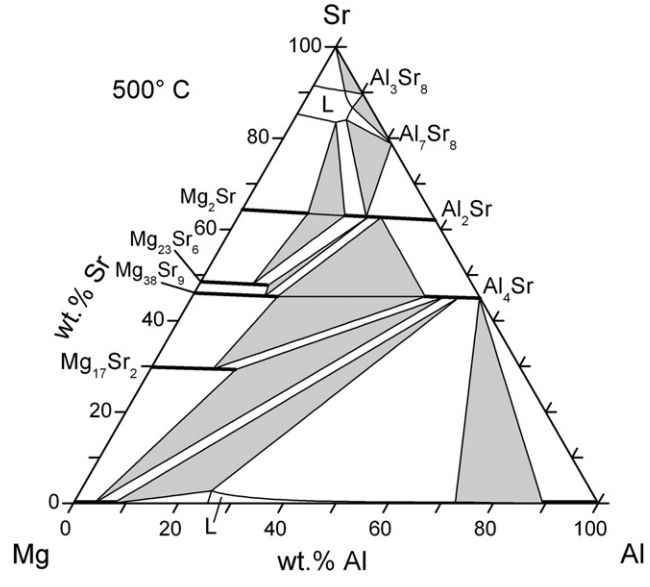

Fig. 4. Isothermal section calculated at 500 °C. The grey areas indicate three-phase regions. The ternary phase τ does not exist at 500 °C.

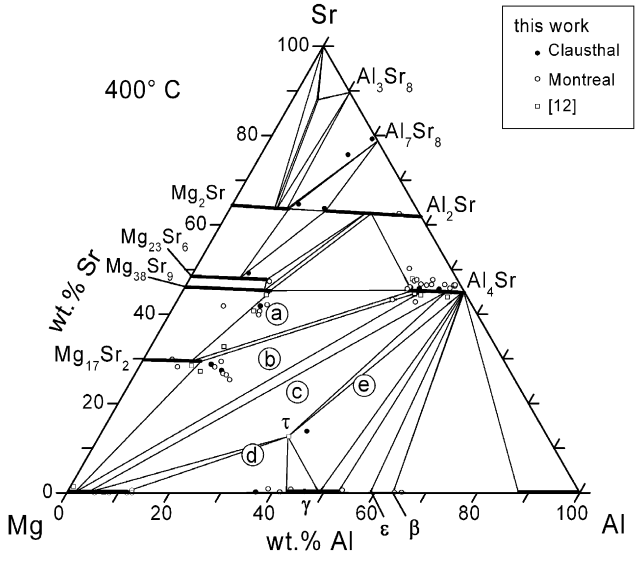

Fig. 5. Isothermal section calculated at 400 °C. Small dots show room temperature EPMA data including data from Ref. [12]. The three-phase regions marked with characters (a)–(e) correspond to the micrographs in Fig. 1(a)–(e). Calculated equilibria > 70 wt% Sr are not supported by experimental data.

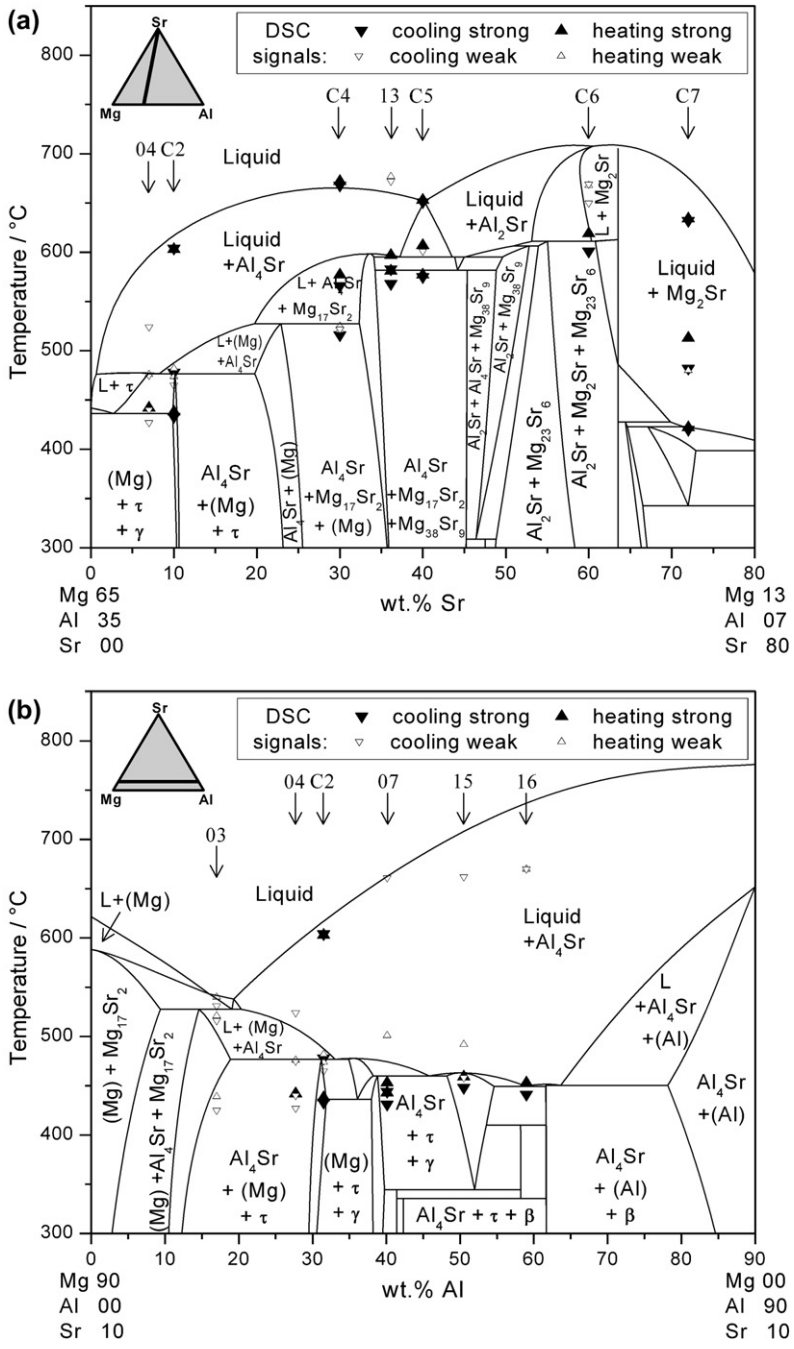

Fig. 6. Calculated vertical phase diagram section (a) from $Mg_{65}Al_{35}$ to the Sr-corner and (b) at constant 10 wt% Sr compared with experimental data from DSC analysis.

at 400 °C. Again the large primary Al_4Sr-blocks are obvious. $Mg_{17}Sr_2$ is the secondary phase solidified in concave shape adjacent to these blocks. Finally, the precipitation of $(Mg) + Al_4Sr$ in fine lamellar texture is observed, formed in the reaction U4: $L + Mg_{17}Sr_2 = (Mg) + Al_4Sr$. The entire equilibrium solidification sequence was calculated in a similar fashion as in Fig. 8 for this and the following samples, supporting these conclusions. It is noteworthy that again the transition type reaction runs to completion and terminates solidification in this sample. In a more rapid (non-equilibrium) solidification, one should expect incomplete reaction at U4 − and also the following U5 − with residual liquid reaching the eutectic E4, see Fig. 3b. That can be shown by a calculation under Scheil conditions and in this case additional phases τ and γ are expected. These phases could not be observed in the microstructure, compounding the equilibrium solidification of this sample in accord with the thermodynamic calculation, even though the thermal signals of secondary and tertiary reactions are somewhat below the calculation, see Fig. 6a. Nevertheless, the actual occurrence of an invariant reaction U4 is also supported by the thermal data.

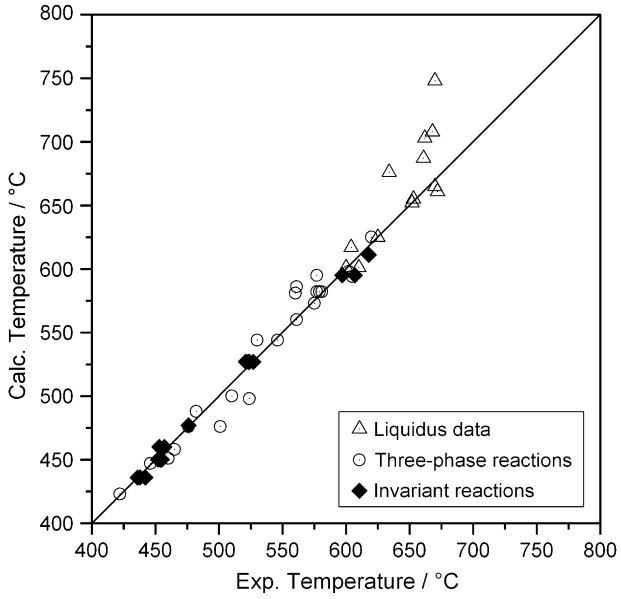

Fig. 7. Comparison between calculated results and all experimental thermal analysis data from Tables 1 and 3. The straight line is a visual aid corresponding to perfect agreement between experimental values and the calculated results from the present thermodynamic model.

Also in sample 06 (Fig. 1c) primary Al_4Sr precipitates dominate the microstructure as large blocks. Adjacent to these blocks large fields of (Mg) were grown, which is the secondary phase in accord with the calculated monovariant reaction $L = (Mg) + Al_4Sr$. Solidification of this sample should terminate in equilibrium at the reaction U5 with formation of τ in a phase fraction of 20%. This transition type reaction, $L + Al_4Sr = \tau + (Mg)$, is obviously overrun, with substantial amount of residual liquid reaching the ternary eutectic E4, where the fine lamellar structure $(Mg) + \gamma\text{-}Mg_{17}Al_{12}$ is produced. This eutectic structure is almost binary, considering the small Sr-content of 0.024 wt% Sr in the liquid at E4. Taking a closer look at the BSE-image, we can see some areas of a larger grown particle, denoted as τ in the magnified inset, which is different from the lamellar eutectic structure and also brighter than the (Mg) phase. This particle is very close to the color of $\gamma\text{-}Mg_{17}Al_{12}$ but slightly brighter, indicating higher Sr-content. We assume that this is the first appearance of the τ phase, even though these particles are too small for a meaningful EPMA. The kinetics of τ formation seems to be slow, so sample 06 did not fully equilibrate compared to the thermodynamic calculations. This microstructure is in good agreement with the Scheil calculation, indicating a very small amount of τ and a substantial amount of non-equilibrium $\gamma\text{-}Mg_{17}Al_{12}$ phase.

Considering the chemical similarity of Sr and Ca and the reported substantial solubility of 6 at% Ca at 400 °C in $\gamma\text{-}Mg_{17}Al_{12}$ [19], one might suspect that Sr dissolves similarly in $\gamma\text{-}Mg_{17}Al_{12}$. It is shown with sample C2 (Fig. 1d) that this suspicion is not true and, moreover, that a distinct ternary phase τ exists, which is not just a ternary solubility of Sr in $\gamma\text{-}Mg_{17}Al_{12}$. The solidification of this sample starts with the primary block Al_4Sr and the secondary growth of (Mg) next to it, so far obeying equilibrium conditions. At 477 °C all of the primary Al_4Sr should be entirely consumed in the U5 reaction, $L + Al_4Sr = \tau + (Mg)$, forming a huge amount of 78% of τ. Again, this reaction does not run to complete equilibrium, especially for the large blocks of Al_4Sr. The reaction type, however, is supported by the microstructure in Fig. 1d, showing small residuals of white Al_4Sr spots enclosed by τ adjacent to (Mg). A Scheil calculation for the same alloy demonstrates that, after overrunning U5, a small amount of only 7% of τ is formed during the monovariant eutectic reaction $L = \tau + (Mg)$, located between U5 and E4 in Fig. 3b. Such

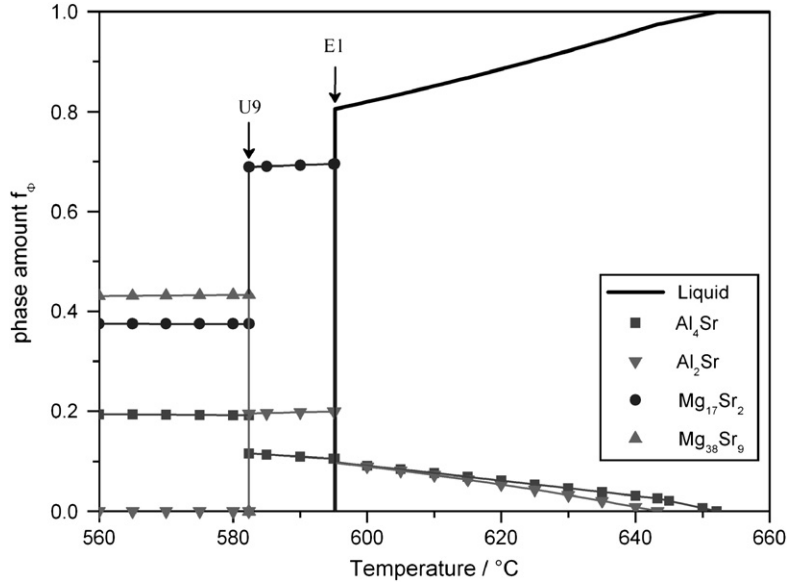

Fig. 8. Phase amounts (atomic fractions) calculated for solidification under equilibrium conditions for sample C5, see Fig. 1(a). U9 is a solid state reaction, $Mg_{17}Sr_2 + Al_2Sr = Al_4Sr + Mg_{38}Sr_9$.

a small amount of τ is quite consistent with the microstructure in Fig. 1d, showing also the perfect agreement with the subsequent ternary eutectic solidification at E4, with the fine lamellar (Mg) + γ-$Mg_{17}Al_{12}$ structure and negligible amount of τ. The mass contrast produced by the back scattered electrons clearly distinguishes τ (light grey, higher Sr-content) and γ-$Mg_{17}Al_{12}$ (dark grey, lower Sr-content) as separate phases. In the large particles of τ the substantial Sr-content was quantitatively analyzed with EPMA to be ~13.5 wt% Sr. The measured Mg/Al ratio of τ is 46.5/40 wt%, which is very similar to that of γ-$Mg_{17}Al_{12}$. Even though the γ-$Mg_{17}Al_{12}$ phase is too finely distributed in Fig. 1d for a meaningful point analysis, its negligible Sr-solubility is demonstrated by the EPMA X-ray map of the fine lamellar two-phase (Mg) + γ-$Mg_{17}Al_{12}$ region shown in Fig. 2. This compounds the negligible Sr-solubility in *both* phases, (Mg) and γ-$Mg_{17}Al_{12}$. The approximate molar composition of the ternary phase τ, $Al_{38}Mg_{58}Sr_4$, was assigned according to the EPMA data of large single phase particles; it is not related to a crystal structure, which is unknown. There is some scatter in the EPMA data of τ measured at different points; as an average value, also considering the data of Ref. [12], 12.6 wt% Sr, 50.4 wt% Mg and 37 wt% Al was finally assessed. The fixed stoichiometry of τ may be a simplification.

The mass contrast distinction between the phases τ and γ-$Mg_{17}Al_{12}$ is also demonstrated in sample 08 (Fig. 1e). After the primary solidification of the Al_4Sr-bars the thermodynamic calculation indicates a secondary monovariant peritectic reaction, $L + Al_4Sr = \tau$. This equilibrium reaction occurs over the narrow temperature range of 473–460 °C, producing about 36% of τ phase while nibbling off Al_4Sr from the primary amount of 42% down to 35%. This peritectic reaction type is in perfect agreement with Fig. 1e, showing a peripheral rim of τ around all Al_4Sr crystals. This peritectic reaction ends at U6, see also Fig. 3b, where the equilibrium solidification ends in a production of a large amount of γ-$Mg_{17}Al_{12}$ and some τ. This calculation is in excellent agreement with the microstructure in Fig. 1e. Only a very small amount of Al_4Sr needs to be consumed in this reaction at 460 °C, $L + Al_4Sr = \tau + \gamma$, and this is probably the reason for the near-equilibrium completion of this reaction. By contrast, a Scheil calculation for that alloy predicts roaming of a residual liquid down to E4, where 7% of (Mg) should form, in addition to the large amount of γ. A small amount of such eutectic (Mg)-precipitates might be present in the sample, e.g. in the area between the two marks of τ; the black spots above that area in Fig. 1e are holes.

6. Conclusion

- The discrepancies in the experimental data in the ternary system Al–Mg–Sr concerning the existence of ternary phases or solubilities reported by Makhmudov et al. [6–10] and Parvez et al. [11] could be solved by investigating six key samples, combined with a more detailed evaluation of the complete raw experimental information of Ref. [11].
- Substantial mutual solid solubilities of Al in binary Mg–Sr compounds and of Mg in binary Al–Sr compounds exist. The suspected Sr-solubility in γ-$Mg_{17}Al_{12}$ is negligible. Only one distinct ternary phase τ, $Al_{38}Mg_{58}Sr_4$, exists.
- A consistent thermodynamic modeling of the ternary phase equilibria is generated. It is well supported by experimental data in the partial system Mg–Al–Al_2Sr–Mg_2Sr. The most complex equilibria involving the (Mg) phase are studied meticulously. The Sr-rich corner, above ≈70 wt% Sr, is calculated for the sake of completeness. This region is not investigated in more detail in this work because of problems in sample preparation and its insignificance for Mg- or Al-based alloys.
- The evolution of microstructures during slow solidification (5 and 1 K/min) is analyzed by detailed thermodynamic calculations for five samples representing different important phase sequences. This analysis goes beyond the calculated phase diagrams and the liquidus surface. The kinetics of formation of the ternary phase τ is apparently slow; the corresponding microstructures are best understood applying non-equilibrium Scheil calculations. The formation of τ is verified both in a partly occurring four-phase transition type reaction, U5, and in a monovariant peritectic reaction, $L + Al_4Sr = \tau$. By contrast, the invariant reaction involving the Mg-richest liquid, U4, proceeds in near-equilibrium, even though it is also of the transition type. The good agreement with all of the experimental microstructures provides additional support for the thermodynamic description generated in this work.

Acknowledgements

The authors are grateful to Elhachmi Essadiqi and Jian Li of CANMET, Ottawa, Canada, for providing additional EPMA and SEM data. YAC wishes to thank NSF through the FRG Grant No. DMR-0309468 and Wisconsin Distinguished Professorship for financial support. This study is supported by the German Research Foundation (DFG) in the Priority Programme "DFG-SPP 1168: InnoMagTec" under grant no. Schm 588/27(29).

References

[1] Luo AA. Recent magnesium alloy development for elevated temperature applications. Int Mater Rev 2004;49:13–30.
[2] Baril E, Labelle P, Pekguleryuz MO. Elevated temperature Mg–Al–Sr: creep resistance, mechanical properties, and microstructure. JOM 2003;55:34–9.
[3] Pekguleryuz MO, Kaya AA. Creep resistant magnesium alloys for powertrain applications. Adv Eng Mater 2003;5(12):866–78.
[4] Czerwinski F, Zielinska-Lipiec A. The microstructure evolution during semisolid molding of a creep-resistant Mg–5Al–2Sr alloy. Acta Mater 2005;53:3433–44.
[5] Chartrand P, Pelton AD. Critical evaluation and optimization the thermodynamic properties and phase diagrams of the Al–Mg, Al–Sr, Mg–Sr, and Al–Mg–Sr systems. J Phase Equilib 1994;15(6):591–605.
[6] Makhmudov MM, Vakhobov AV, Dzhuraev TD, Ganiev IN. Combined solubility of components of a magnesium–aluminum–strontium system

in aluminum- and magnesium-rich regions. Dokl Akad Nauk Tadzh SSR 1980;23(1):25–8.
[7] Makhmudov MM, Vakhobov AV, Dzhuraev TD. Liquidus surface of aluminum and magnesium phases of the magnesium–aluminum–strontium diagram. Dokl Akad Nauk Tadzh SSR 1981;24(7):435–8.
[8] Makhmudov MM, Bodak OJ, Vakhobov AV, Dzhurayev TD. Phase equilibria in the Mg–Al–Sr system. Izv Akad Nauk SSSR Met 1981;6: 209–12.
[9] Makhmudov MM, Vakhobov AV, Dzhuraev TD. Examination of quasibinary sections of the Mg–Al–Sr system. Russ Metal 1982;1: 122–4.
[10] Makhmudov MM, Vakhobov AV, Ganiev IN. Study of the liquidus surface of the Sr/SrMg(SrMg(2))/Sr–Al(SrAl(4)) system using simplex experimental planning. Zavod Lab 1982;48:61–2.
[11] Parvez MA, Medraj M, Essadiqi E, Dénès G. Experimental study of the ternary magnesium–aluminium–strontium system. J Alloys Compd 2005;402:170–85.
[12] Cao H, Zhu J, Zhang C, Wu K, Saddock ND, Jones JW, et al. Experimental investigation and thermodynamic modeling of the Mg–Al rich region of Mg–Al–Sr system. Z Metallkd 2006;97:422–8.
[13] Kraus W, Nolze G. Powdercell for Windows, version 2.4. Berlin, Germany, Federal Institute for Materials Research and Testing, <http://www.bam.de/service/publikationen/powdercell_i.htm>.
[14] Liang P, Tarfa T, Robinson JA, Wagner S, Ochin P, Harmelin MG, et al. Experimental investigation and thermodynamic calculation of the Al–Mg–Zn system. Thermochim Acta 1998;314:87–110.
[15] Zhong Y, Wolverton C, Austin Chang Y, Liu Z-K. A combined CALPHAD/first-principles remodeling of the thermodynamics of Al–Sr: unsuspected ground state energies by ''rounding up the (un)usual suspects''. Acta Mater 2004;52:2739–54.
[16] Zhong Y, Sofo JO, Luo AA, Liu Z-K. Thermodynamics modeling of the Mg–Sr and Ca–Mg–Sr systems. J Alloys Compd 2006;421:172–8.
[17] Dinsdale AT. SGTE data for pure elements. Calphad 1991;15:317–425.
[18] Hillert M. The compound energy formalism. J Alloys Compd 2001;320:161–76.
[19] Suzuki A, Saddock ND, Jones JW, Pollock TM. Solidification paths and eutectic intermetallic phases in Mg–Al–Ca ternary alloys. Acta Mater 2005;53(9):2823–34.
[20] Villars P, Calvert LD. Pearson's handbook of crystallographic data for intermetallic phases. 2nd ed. Metals Park, Ohio: ASM International; 1991.
[21] Massalski TB, Okamoto H, Subramanian PR, Kacprzak L, editors. Binary alloy phase diagrams. 2nd ed. Metals Park, Ohio: ASM International; 1990.
[22] Su H-L, Harmelin M, Donnadieu P, Baetzner C, Seifert HJ, Lukas HL, et al. Experimental investigation of the Mg–Al phase diagram from 47–63 at.% Al. J Alloys Compd 1997;247:57–65.